

## Anyonic bound states in the continuum

Weixuan Zhang <sup>1,3</sup>, Long Qian<sup>1,3</sup>, Houjun Sun <sup>2</sup> & Xiangdong Zhang <sup>1</sup>✉

Bound states in the continuum (BICs), which are spatially localized states with energies lying in the continuum of radiating modes, are discovered both in single- and few-body systems with suitably engineered spatial potentials and particle interactions. Here, we reveal a type of BICs that appear in anyonic systems. It is found that a pair of non-interacting anyons can perfectly concentrate on the boundary of a one-dimensional homogeneous lattice when the statistical angle is beyond a threshold. Such a bound state is embedded into the continuum of two-anyon scattering states, and is called as anyonic BICs. In contrast to conventional BICs, our proposed anyonic BICs purely stem from the statistics-induced correlations of two anyons, and do not need to engineer defect potentials or particle interactions. Furthermore, by mapping eigenstates of two anyons to modes of designed circuit networks, the anyonic BICs are experimentally simulated by measuring spatial impedance distributions and associated frequency responses. Our results enrich the understanding of anyons and BICs, and can inspire future studies on exploring correlated BICs with other mechanisms.

<sup>1</sup>Key Laboratory of advanced optoelectronic quantum architecture and measurements of Ministry of Education, Beijing Key Laboratory of Nanophotonics & Ultrafine Optoelectronic Systems, School of Physics, Beijing Institute of Technology, 100081 Beijing, China. <sup>2</sup>Beijing Key Laboratory of Millimeter wave and Terahertz Techniques, School of Information and Electronics, Beijing Institute of Technology, 100081 Beijing, China. <sup>3</sup>These authors contributed equally: Weixuan Zhang, Long Qian. ✉email: [zhangxd@bit.edu.cn](mailto:zhangxd@bit.edu.cn)

**B**ound states in the continuum (BICs) were originally proposed for electrons in a peculiar quantum mechanical potential by von Neumann and Wigner in 1929<sup>1</sup>, and were later revealed to be a general phenomenon for both quantum and classical waves<sup>2,3</sup>. As for single-particle systems and their classical analogies, various mechanisms could be used to produce BICs. For example, the coupling of certain resonances to radiation modes could be forbidden by symmetry or separability, which are called symmetry-protected BICs or separable BICs<sup>4–8</sup>. In addition, it is also possible to suppress radiations into all channels by tuning a finite number of systematical parameters<sup>9–18</sup>. This suppression can always be interpreted as a result of the destructive interference of multiple radiating components. Moreover, instead of looking for the presence of BICs in a given system, we can also inversely design a system by engineering the potential, the hopping rate or the boundary shape of the system to construct BICs<sup>19–21</sup>. It is found that BICs proposed in classical-wave systems could have large quality-factors and extremely enhanced near-field concentrations. These superior properties give many important applications based on BICs, such as the ultralow threshold BIC-laser<sup>10,22,23</sup>. While, single-particle BICs are always fragile objects, which appear in artificial systems with specific designs. In this case, finding other robust ways to create BICs is of great significance.

On the other hand, except for the widely discussed single-particle system, many investigations have shown that the correlated few-body BICs can also exist in the two-boson Hubbard model by engineering the onsite interaction and impurity potential at bulk or boundary site<sup>24,25</sup>. In particular, two-boson bulk BICs could appear when the absolute value of impurity potential on the bulk site is larger than that of the Hubbard interaction, which is required to possess the same sign with the impurity potential on the bulk site<sup>24</sup>. As for the correlated two-boson model with a boundary impurity potential, it is shown that Tamm–Hubbard BICs require an infinitesimally-small value of the boundary impurity potential, which has the opposite sign with respect to the Hubbard interaction<sup>25</sup>. Different from most single-particle BICs that need specific designs in artificial systems, the two-boson BICs always exist in a wide range of interaction strengths and defective potentials. It can move into and out of the continuum continuously by tuning these parameters, making two-particle BICs become robust and tunable. Taken together, the currently proposed single- and few-body BICs are all based on the engineering of systematic symmetries, potential and material distributions, or particle-particle interactions. Exploring new mechanisms for the generation of BICs is still an important problem in the field of physics and material sciences.

In this work, we demonstrate both theoretically and experimentally that BICs can be purely induced by quantum statistics. Such a type of BICs can exist in anyonic systems with the statistical angle exceeding a threshold. Anyons are quantum quasi-particles with statistics intermediate between bosons and fermions<sup>26–40</sup>. The existence of anyons was predicted in the 1980s, and the strong experimental evidence of anyons has emerged recently<sup>33,34</sup>. It is widely known that anyons could play important roles in several areas of modern physics research, such as fractional quantum Hall systems<sup>35</sup>, spin liquids<sup>36</sup> and topological quantum computations<sup>37</sup>. Meanwhile, some recent investigations have shown that quantum statistics could trigger the appearance of many interesting effects, such as anyonic Bloch oscillations<sup>38,39</sup> and topological transitions<sup>40</sup>. Beyond these novel physical phenomena, here, we reveal that exotic BICs can also exist in non-interacting anyonic systems. Moreover, using the exact mapping of two anyons in the finite one-dimensional lattice to modes of the two-dimensional circuit, anyonic BICs are experimentally emulated. Our work opens the

door to novel physics induced by the interplay between BICs and anyons.

## Results

**The theory of anyonic bound states in the continuum.** We start by considering a pair of non-interacting anyons (marked by two letters of ‘*m*’ and ‘*n*’) hopping on a one-dimensional (1D) chain with open boundaries, as shown in Fig. 1a. In this case, the system can be described by the tight-binding lattice model as:

$$H = -J \sum_{l=1}^{L-1} (\hat{a}_l^+ \hat{a}_{l+1} + \hat{a}_{l+1}^+ \hat{a}_l) \quad (1)$$

where  $\hat{a}_l^+$  ( $\hat{a}_l$ ) is the creation (annihilation) operator of the anyon at the *l*th lattice site. *L* is the length of 1D lattice, and *J* is the single-particle hopping rate. In the following, we always set *J* = 1. The anyonic creation and annihilation operators obey commutation relations as  $\hat{a}_k^+ \hat{a}_l - \hat{a}_l^+ \hat{a}_k e^{i\theta \text{sgn}(l-k)} = \delta_{lk}$  and  $\hat{a}_l \hat{a}_k - \hat{a}_k \hat{a}_l e^{i\theta \text{sgn}(l-k)} = 0$ , where  $\theta$  is the anyonic statistical angle and  $\text{sgn}(x)$  equals to  $-1$ ,  $0$  and  $1$  for  $x < 0$ ,  $x = 0$  and  $x > 0$ , respectively. Based on the commutation relation, we note that two anyons on the same lattice site behave as ordinary bosons. In this case, anyons with  $\theta = \pi$  (always called as pseudofermions<sup>32</sup>) could be regarded as bosons when they occupy the same site and ordinary fermions when they occupy different sites. The two-anyon solution can be expanded in Fock space as  $|\psi\rangle = \frac{1}{\sqrt{2}} \sum_{n,m=1}^L c_{nm} \hat{a}_n^+ \hat{a}_m^+ |0\rangle$ , where  $|0\rangle$  is the vacuum state and  $c_{nm}$  is the probability amplitude with one anyon at site *m* and the other one at site *n*. Under the restriction of anyonic statistics, the equality of  $c_{nm} = e^{i\theta \text{sgn}(n-m)} c_{mn}$  is satisfied. By solving the steady-state Schrödinger equation  $H|\psi\rangle = \varepsilon|\psi\rangle$  of two anyons, the corresponding eigenequation with respect to  $c_{nm}$  can be described by:

$$\varepsilon c_{nm} = -J [e^{i\theta(\delta_{n,m} + \delta_{n,m-1})} c_{n(m-1)} + e^{-i\theta(\delta_{n,m} + \delta_{n,m+1})} c_{n(m+1)} + c_{(n-1)m} + c_{(n+1)m}] \quad (2)$$

The mode coupling of two anyons determined by Eq. (2) can be illustrated in the 2D Fock space, as shown in Fig. 1b. The site located at (*n*, *m*) represents the two-anyon state of  $c_{nm}$ . In this case, the site enclosed by the black (blue) dash block corresponds to the state with the first (second) anyon locating at *n* = 3 (*n* = 4) and the second (first) anyon locating at *m* = 4 (*m* = 3), as presented in Fig. 1a. Solid lines and arrows represent real-valued hopping strengths (*J*) and complex-valued hopping strengths ( $J e^{\pm i\theta}$ ), respectively. It is shown that anyonic statistics can only introduce complex couplings around diagonals (blue sites with *n* = *m* and *n* = *m* ± 1). Away from diagonals (black sites with  $|n - m| > 1$ ), the mode couplings are real-valued.

The above eigenequation of two anyons can be solved analytically by assuming a Bethe-type ansatz of two-anyon state as  $c_{nm}(k_n, k_m, A_{i=1,\dots,8})$ <sup>24,25</sup>, which is in the form of a superposition with eight plane waves (see Supplementary Note 1 for details). Here,  $k_m$  and  $k_n$  are a pair of complex wave numbers related to two anyons, and  $A_1$  to  $A_8$  are amplitudes of eight plane waves. We note that the eigenequation should be written in different forms with the considered lattice site locating at diagonals and off diagonals of the two-anyon Fock space. Hence, we handle these two cases separately to solve the two-anyon eigenequation.

At first, we substitute  $c_{nm}(k_n, k_m, A_{i=1,\dots,8})$  into the steady-state eigenequation away from diagonals. It is found that the eigenenergy of two distant anyons could be written as  $\varepsilon = -2\cos(k_m) - 2\cos(k_n)$ . It manifests that energies of two-anyon scattering states are always ranging from  $-4$  to  $4$ . Then, we

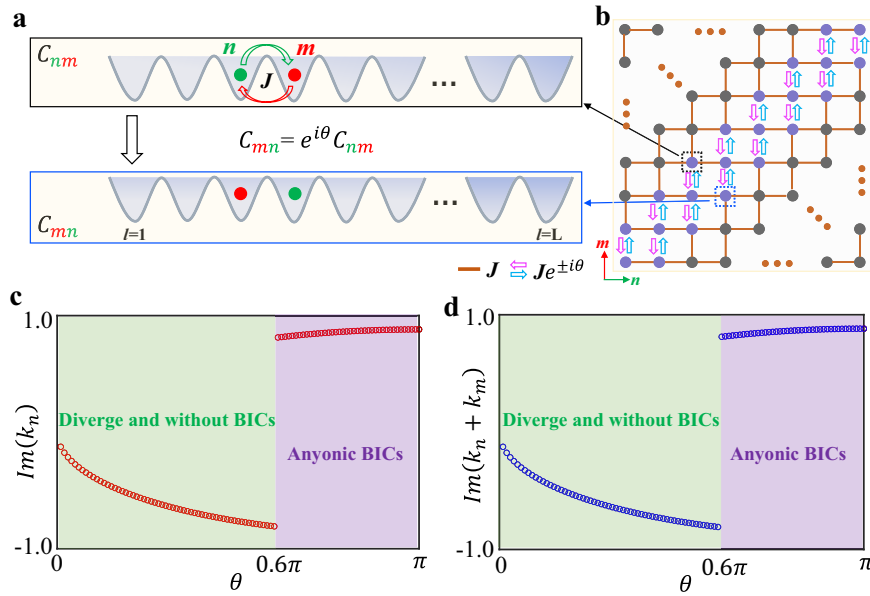


**Fig. 1 Analytical results for the two-anyon bound states in the continuum (BICs).** **a** The schematic diagram for the 1D lattice model possessing two anyons with the statistical angle marked by  $\theta$ . **b** The scheme of the two-anyon Fock space. Solid lines and arrows represent real-valued hopping strengths and complex-valued hopping strengths, respectively. Two-anyon modes enclosed by black and blue dash blocks are presented in Fig. 1a. **c** and **d** The variations of  $Im(k_n)$  and  $Im(k_m + k_n)$  as functions of the anyonic statistical angle. Here, the two-anyon state is assumed in the form of  $c_{nm} = A_1 \exp(ik_n n + ik_m m)$  with  $n \geq m$ . The purple (green) region corresponds to the range of statistical angle, where non-diverge BICs are supported (unsupported) in the two-anyon system. Here,  $k_m$  and  $k_n$  are a pair of complex wave numbers related to two anyons.

substitute  $c_{nm}(k_n, k_m, A_{i=1,\dots,8})$  into the steady-state eigenequation at diagonals. In this case, a set of linear equations related to  $A_1$  to  $A_8$  are obtained. These linear equations could be expressed in a matrix form as  $M_{ij}A_j = 0$  ( $i, j = 1, \dots, 8$ ), where  $M$  is an 8 by 8 matrix (see Supplementary Note 1 for details). Through the direct computation, we find that the determinant of matrix  $M$  satisfies  $det(M) = 0$ . This means that the two-anyon solution is admitted for any complex values of  $k_m$  and  $k_n$  accompanied with suitable values of  $A_j$  ( $j = 1, \dots, 8$ ). The only limitation on  $k_m$  and  $k_n$  is the non-diverge requirement of  $c_{nm} \rightarrow 0$  with  $n, m \rightarrow \infty$ .

Based on the solvability condition for the matrix equation  $M_{ij}A_j = 0$ , we can assume the Bethe-type ansatz of two anyons in a simple form as  $c_{nm} = A_1 \exp(ik_n n + ik_m m)$  with  $n \geq m$ . Substituting this simplified two-anyon state into the steady-state eigenequation at diagonals, two complex wave-vectors  $k_n$  and  $k_m$  can be expressed by the statistical angle  $\theta$  as  $z_n = -(-e^{i\theta} + e^{2i\theta} \pm \sqrt{-e^{i\theta} + 3e^{2i\theta} - 3e^{3i\theta} + e^{4i\theta}})/(\sqrt{1 - e^{i\theta}} \sqrt{(-1 + e^{i\theta})e^{i\theta}})$  and  $z_m = \pm \sqrt{1 - e^{i\theta}}/\sqrt{-e^{i\theta} + e^{2i\theta}}$  with  $z_n = \exp(-ik_n)$  and  $z_m = \exp(-ik_m)$  (see Supplementary Note 2 for details). We note that the assumed two-anyon state can be re-expressed as  $c_{nm} = A_1 \exp[ik_n(n - m) + i(k_m + k_n)m]$  with  $n \geq m$ . In this case, such a two-anyon state can meet the non-diverge requirement and become a perfect bound state if two wave-vectors satisfy relations of  $Im(k_n) > 0$  and  $Im(k_m + k_n) > 0$ .

To get the required value of  $\theta$  for the appearance of two-anyon bound states, the variations of  $Im(k_n)$  and  $Im(k_m + k_n)$  as a function of the statistical angle  $\theta$  are calculated, as shown in Fig. 1c and d. We can see that a sudden change of  $Im(k_m + k_n)$  and  $Im(k_n)$  from negative (the green region) to positive (the purple region) appears when the statistical angle is beyond  $0.6\pi$ . This indicates that the perfect bound state only appears when the value of statistical angle exceeds the threshold ( $\theta = 0.6\pi$ ). In addition, the effective on-site potential is uniform, and the

absolute value of the coupling strength is also fixed to a constant in the mapped 2D lattice. Hence, eigen-energies of two-anyon bound states should always lie into the continued energy-spectrum of two-anyon scattering states, making perfect bound states of two anyons become anyonic BICs (see numerical demonstrations in the following).

An intuitive understanding for the existence of anyonic BICs with a threshold of  $\theta$  can be illustrated by the competition between statistics-induced localizations and free hoppings of anyons. Specifically, complex couplings induced by quantum statistics can generate a defective potential on corners of two-anyon Fock space. The larger the statistical angle is, the deeper the defective potential becomes. When the strength of defective potential can suppress the role of two-anyon free hoppings, localized two-anyon BICs appear.

To demonstrate the above analytical prediction of anyonic BICs, we numerically calculate the inverse participation ratio (IPR)<sup>41</sup>, which is defined by  $IPR = \sum_{m,n} |C_{nm}|^4$ , to qualify the localization of two-anyon eigenstates. As shown in Fig. 2a, the variation of IPRs of all two-anyon eigenmodes as a function of the statistical angle is calculated. The lattice length is set as  $L = 171$ . It is seen that a large ratio of two-anyon eigenstates (black dots) possess near-zero IPRs, corresponding to the extended two-anyon scattering states. There are also two types of anyonic eigenstates with relatively large IPRs, as marked by blue and red lines. But, these two types of two-anyon states show different behaviors with the change of  $\theta$ . The mode marked by the blue line always exists at different values of  $\theta$ . While, IPRs of two-anyon modes marked by the red line increase significantly when the value of  $\theta$  exceeds  $0.6\pi$  (as illustrated by the purple region). It indicates that this type of two-anyon states exhibit the enhanced localization with  $\theta$  exceeding a threshold.

To justify whether these two types of localized anyonic modes are perfect bound states, we calculate the evolution of IPRs as a function of the lattice length in Fig. 2b and c with the statistical angle being

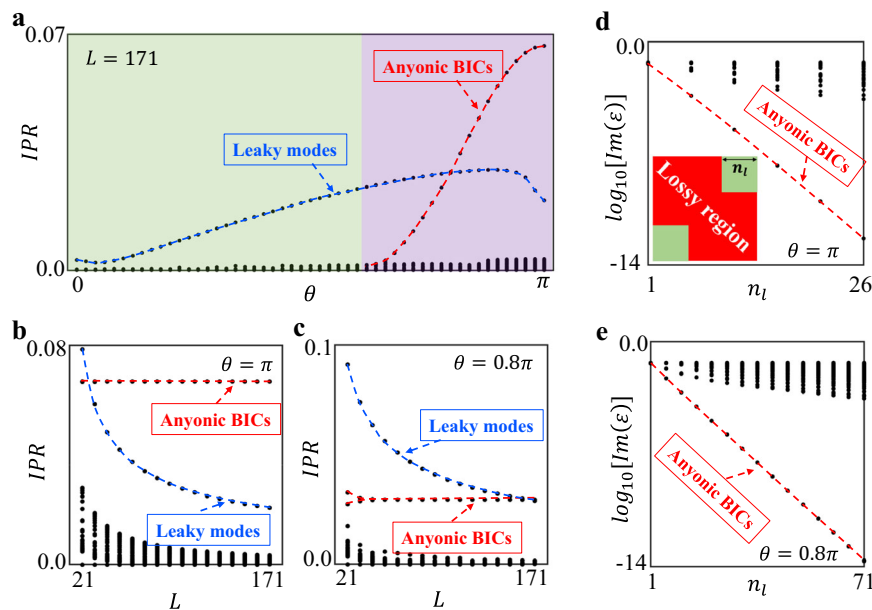


**Fig. 2 Numerical results for the demonstration of two-anyon bound states in the continuum (BICs).** **a** The calculated inverse participation ratios of all two-anyon eigenstates with  $L = 171$  at different anyonic statistical angles. Red and blue dash lines are used to mark two types of anyonic modes with large inverse participation ratios (IPRs). **b** and **c** The evolution of IPRs for two-anyon eigenmodes as a function of the lattice length with the statistical angles being  $0.8\pi$  and  $\pi$ , respectively. **d** and **e** Numerical results on the variation of imaginary parts of eigen-energies as a function of the size for the lossless region, where the statistical angles are set as  $\theta = \pi$  and  $\theta = 0.8\pi$ , respectively. The inset of **(d)** plots the schematic diagram for the region with artificial losses.

$\theta = 0.8\pi$  and  $\theta = \pi$ , respectively. It is clearly shown that IPRs of two-anyon eigenstates marked by blue lines decrease significantly with the lattice size being increased, indicating that those states are leaky modes and could couple with two-anyon scattering states. While, IPRs of anyonic modes marked by red lines are saturated with increasing the lattice size, manifesting the perfect localization of these eigenmodes at both statistical angles. The splitting of eigenenergies of two-anyon bound states at  $\theta = 0.8\pi$  is due to the finite size effect, where the two-anyon bound states at two corners  $(1, 1)$  and  $(L, L)$  are coupled with each other. In addition, following another numerical method on the demonstration of BICs<sup>42,43</sup>, we further calculate the scaling of imaginary part of two-anyon eigen-energies by changing the size of the lattice region with artificial losses. The artificial losses are introduced by adding the non-Hermitian on-site term  $(0.05i)$  to some lattice sites, which are inside the red area of the mapped 2D lattice model plotted in the inset of Fig. 2d. Here, the size of lossless region is marked by  $n_l$ . Fig. 2d and 2e present numerical results on the variation of imaginary parts of two-anyon eigen-energies as a function of  $n_l$ . Here, the statistical angles are set as  $\theta = \pi$  (in Fig. 2d) and  $\theta = 0.8\pi$  (in Fig. 2e), respectively. The lattice length equals to  $L = 171$ . We can see that imaginary components of eigen-energies for anyonic BICs (corresponding to modes marked by red lines in Fig. 2a–c) approach to zero in an exponential scaling with increasing the size of the lossless region. This phenomenon further demonstrates the correctness of the existence of anyonic BICs.

Furthermore, as shown in Fig. 3a–e, we calculate eigenenergies of two anyons with  $\theta = \pi, 0.8\pi, 0.7\pi, 0.6\pi$  and  $0.5\pi$  ( $L = 171$ ), respectively. Insets correspond to enlarged views of eigen-spectra (enclosed by red blocks) sustaining BIC-related two-anyon states. It is worth noting that the two-anyon eigen-spectra at different statistical angles are all chiral symmetric. In this case, the anyonic BICs should exist at a pair of positive and negative energies with equal absolute values, as marked by solid and dash blocks in Fig. 3a–e. Here, we focus on anyonic BICs with negative energies, and positive-energy counterparts possess identical properties. In Fig. 3f–j, we plot spatial distributions of BIC-related eigenmodes (enclosed by green circles in insets) at different statistical angles.

It is clearly shown that two-anyon states are perfectly concentrated around two corners in the two-anyon Fock space with  $\theta > 0.6\pi$ . The larger the statistical angle is, the stronger the localization of anyonic BICs becomes. In contrast, the two-anyon eigenstates are leaky modes with  $\theta \leq 0.6\pi$ . In addition, we can see that anyonic bound states are lying in the continuum of two-anyon scattering states with  $\theta > 0.6\pi$ . These numerical results clearly verify that the two-anyon bound states are indeed anyonic BICs.

It is worthy to note that the physical origin for the formation of anyonic BICs is different from that of two-boson BICs<sup>24,25</sup>. To construct two-body BICs without single-body analogies, the effective two-body correlation is prerequisite. In theory, the most common two-body correlation is resulting from the Hubbard interaction, which could induce the formation of two-boson BICs. On the other hand, quantum statistics can also induce an effective correlation of two anyons, which is the origin for the formation of anyonic BICs in our system. In addition, we want to stress that the formation of anyonic BICs does not need the existence of the defective potential, but two-boson BICs induced by the Hubbard interaction must require a suitable value of the defective potential.

The requirement of the defective potential for two-boson boundary BICs can be analogized to Tamm surface states of truncated crystals, where the surface potential exceeding a threshold is required. In this case, the defective potential in two-boson systems could be regarded as the effective surface potential of the mapped 2D lattice. As for the two-anyon system, quantum statistics could induce effective defects at two corners in the mapped 2D lattice, which could trap two anyons to form anyonic BICs. Moreover, we can also understand this phenomenon from a mathematical viewpoint. Following the analytical method by assuming a Bethe-type ansatz of two-anyon state, the requirement on the existence of two-body BICs can be derived by expressing two wave numbers ( $k_n$  and  $k_m$ ) with intrinsic parameters of the system, including the Hubbard interaction, the defective potential and the statistical angle. To separately express two wave numbers, two

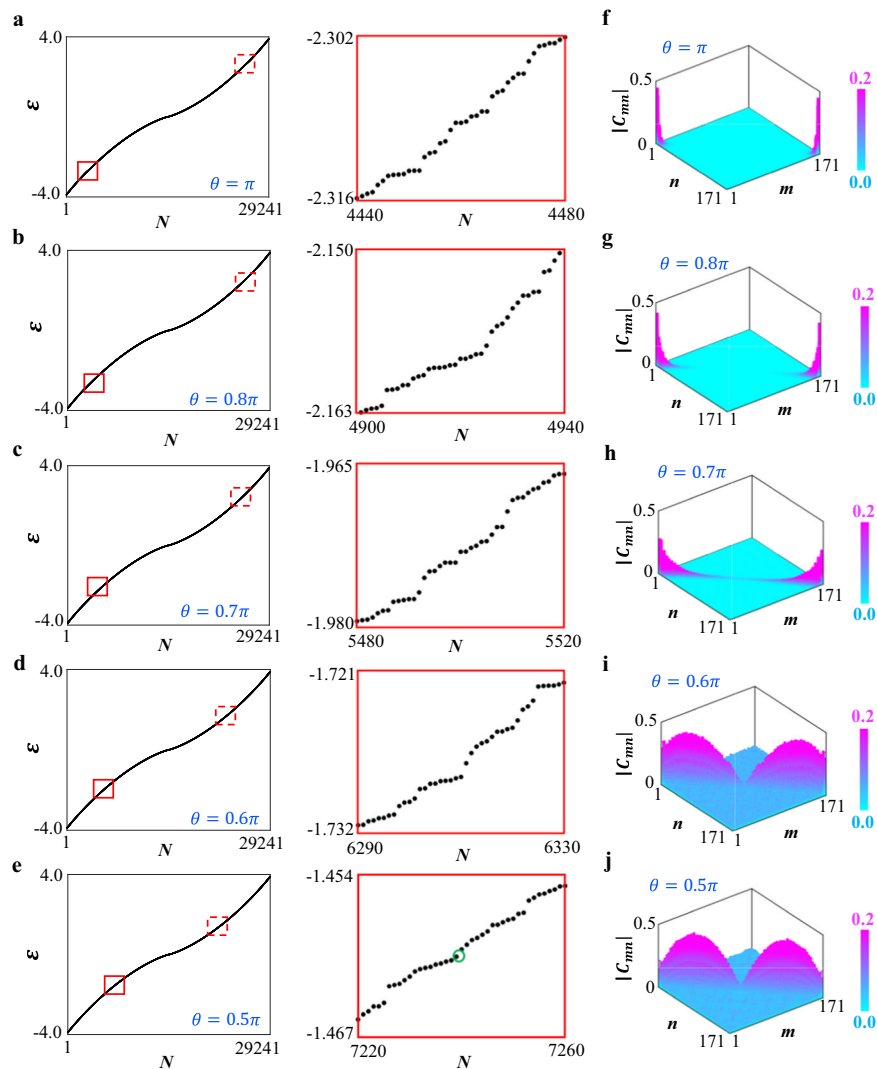


**Fig. 3 Numerical results of eigen-spectra and spatial profiles of localized two-anyon states.** **a–e** Calculated eigenenergies of the two-anyon model with  $\theta = \pi, 0.8\pi, 0.7\pi, 0.6\pi$  and  $0.5\pi$ , respectively. Insets plot enlarged views of anyonic eigenmodes related to bound states in the continuum (BICs) with negative energies. Chiral symmetric counterparts with positive energies are marked by red dash blocks. **f–j** Calculated spatial distributions of BIC-related eigenmodes with  $\theta = \pi, 0.8\pi, 0.7\pi, 0.6\pi$  and  $0.5\pi$ , respectively. The mode index of two-anyon states ( $N$ ) is in the range from 1 to  $L^2$  with  $L = 171$ . The color bars quantify the absolute value of probability amplitude.

different equations related to  $k_m, k_n$  must be constructed basing on the eigen-equation of the two-body system. As for the two-boson system without the defective potential, only one equation can be obtained by considering the eigenequation on the diagonal line ( $m = n$ )<sup>24,25</sup>. In this case, to get the other equation, the defective potential must be introduced. While, as for the case of two anyons, two equations can be directly obtained by considering anyonic eigenequations at  $m = n$  and  $m = n \pm 1$  (see Eq. 9 in Supplementary Materials). Hence, two wave numbers can be expressed by the statistical angle, making the statistical angle  $\theta$  solely determine the existence of anyonic BICs.

The experimental observation of our theoretically predicted anyonic BICs in real quantum systems is not an easy task. In the next part, we will construct 2D circuit networks to simulate the statistics-induced anyonic BICs

**Experimental simulation of anyonic bound states in the continuum by 2D circuit networks.** The 1D two-body Fock space possesses a rigorous correspondence to that of a single particle in the mapped 2D lattice. In this case, by mapping the low-

dimensional few-body configuration space to the high-dimensional tight-binding lattice model, the few-body model can be effectively simulated by the single-particle system with high dimensions. In this case, the Fock space of two anyons (shown in Fig. 1b) can be regarded as a two-dimensional lattice model. Specifically, the probability amplitude for the 1D two-anyon model with one anyon at the site  $n$  and the other at the site  $m$  is directly mapped to the probability amplitude for the single particle locating at the site  $(n, m)$  of the 2D lattice. In details, lattice sites on the main diagonal ( $n = m$ ), first two lateral diagonals ( $n = m \pm 1$ ) and other sites ( $|n - m| > 1$ ) correspond to two anyons located at the same site, two nearest-neighbor sites and two distant sites, respectively. The hopping along a certain direction in the mapped 2D lattice represents the hopping of one anyon in the 1D lattice. In this case, the two-anyon eigenequation can be interpreted as an eigenvalue problem for the mapped 2D lattice, manifesting that the behavior of two anyons in the 1D lattice can be effectively simulated by a single particle in the mapped 2D lattice.



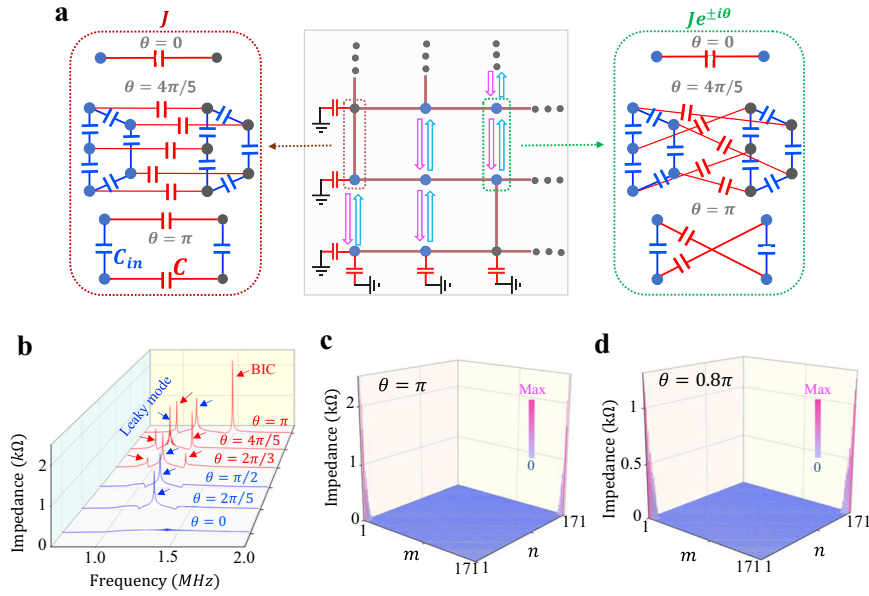


**Fig. 4** The schematic diagram and simulation results of circuit simulators for anyonic bound states in the continuum (BICs). **a** The schematic diagram for the designed circuit simulator for two anyons. Left and right insets illustrate connection patterns for the realization of real-valued and complex-valued coupling strengths with  $\theta = 0, 0.8\pi$ , and  $\pi$ , respectively. **b** The frequency-dependent impedance responses at the left-bottom corner ( $m=1, n=1$ ) of designed electric circuits with different  $\theta$ . Red and blue arrows mark two-anyon BICs and two-anyon leaky modes with large inverse participation ratios (IPRs). **c** and **d** The spatial impedance profiles at frequencies matched to eigenenergies of anyonic BICs with  $\theta = \pi$  and  $0.8\pi$ , respectively. The color bars quantify the absolute value of simulated impedances.

Based on the similarity between the circuit Laplacian and the lattice Hamiltonian<sup>44–54</sup>, electric circuits can be used as a flexible platform to implement the mapped 2D lattice with different statistical angles. To achieve the required complex coupling  $J e^{\pm i\theta}$  around diagonals, circuit pseudospins are needed to be constructed<sup>44,45</sup>. For this purpose, multiple circuit nodes are used to work as a single lattice site, and real and complex hopping rates can be realized by suitably braiding the connection pattern between two groups of circuit nodes, as shown in Fig. 4a. Left and right insets illustrate connection patterns for realizing real-valued and complex-valued coupling strengths, respectively. As for the case with  $\theta = 0$ , one circuit node can work as a single lattice site to fulfill the required real-valued coupling pattern. When the statistical angle equals to  $\theta = 0.8\pi$  ( $\theta = \pi$ ), five (two) circuit nodes, which are connected by capacitors  $C_{in}$  (plotted in blue), are used to form an effective lattice site. In this case, to realize the real-valued hopping rate, capacitors  $C$  (plotted in red) are used to directly link adjacent nodes without a cross, as shown in the left inset. Differently, adjacent circuit nodes are crossly connected via  $C$  to achieve the hopping rate with a phase factor  $e^{\pm i\theta}$  or  $e^{\pm i0.8\theta}$ , as presented in the right inset. In addition, each node is grounded by an inductor  $L_g$ . Through the appropriate setting of grounding and connecting, the circuit eigen-equation can be derived as:

$$\begin{aligned} (f_0^2/f^2 - \nu_\theta C_{in}/C - 4)V_{\downarrow,(n,m)} &= -e^{i\theta(\delta_{n,m} + \delta_{n,m-1})} V_{\downarrow,n(m-1)} \\ &- e^{-i\theta(\delta_{n,m} + \delta_{n,m+1})} V_{\downarrow,n(m+1)} - V_{\downarrow,(n-1)m} - V_{\downarrow,(n+1)m} \end{aligned} \quad (3)$$

where  $f$  is the eigenfrequency ( $f_0 = 1/2\pi\sqrt{CL_g}$ ) of the designed circuit.  $V_{\downarrow,(n,m)}$  represents the voltage of pseudospin at the circuit node  $(n, m)$ , which obeys the statistics-dominated hopping rate.  $\nu_\theta$  is an integer depending on the value of the statistical angle ( $\nu_0 = 1, \nu_{0.8\pi} = 3.618, \nu_\pi = 2$ ). Details for the derivation of circuit eigenequations are provided in Supplementary Note 3. It is shown that the eigen-equation of the designed electric circuit possesses the same form as Eq. (2). In particular, the probability

amplitude for the 1D two-anyon model  $c_{nm}$  is mapped to the voltage of pseudospin  $V_{\downarrow,(n,m)}$  at the circuit node  $(n, m)$ . The eigenenergy ( $\varepsilon$ ) of two anyons is directly related to the eigenfrequency ( $f$ ) of the circuit as  $\varepsilon = f_0^2/f^2 - \nu C_{in}/C - 4$  with  $J = 1$ .

To analyze properties of anyonic BICs in the circuit simulator, we perform circuit simulations using the LTSpice software. Here, the value of  $C, C_{in}$  and  $L_g$  are taken as  $1\text{ nF}, 1\text{ nF}$  and  $3.1\text{ uH}$ , respectively. The simulated 2D circuit networks contain  $171 \times 171$  node groups (corresponding to the 1D two-anyon model with  $L = 171$ ). We note that the impedance response is related to the local density of state of the corresponding quantum tight-binding model<sup>46,47</sup>. Hence, to test whether anyonic BICs exist at expected eigen-energies, we calculate frequency-dependent impedance responses of the corner node ( $m=1, n=1$ ) at different values of  $\theta$ , as presented in Fig. 4b. Here, the effective series resistance of inductance is set as  $50m\Omega$ . It is clearly shown that three significant impedance peaks appear with  $\theta > 0.6\pi$ . The frequencies of two peaks (as marked by red arrows) are matched to positive and negative eigenenergies of two-anyon BICs. We also note that the values (widths) of impedance peak decrease (increase) with the statistical angle changing from  $\pi$  to  $2\pi/3$ . This phenomenon is consistent with the theoretical prediction, where the localization strength of anyonic BICs is largest for two pseudofermions. And, central impedance peaks (marked by blue arrows) correspond to two-anyon leaky modes (marked by the blue line in Fig. 2a), which are not perfect bound states and could couple with two-anyon scattering states. In addition, spatial impedance distributions are further simulated at frequencies corresponding to negative eigenenergies of anyonic BICs with  $\theta = \pi$  (1.448 MHz) and  $\theta = 0.8\pi$  (1.224 MHz), as shown in Fig. 4c and d. We can see that impedance profiles are identical to that of anyonic BICs (shown in Fig. 3f and 3g), demonstrating the correctness of our designed anyonic circuit simulators.

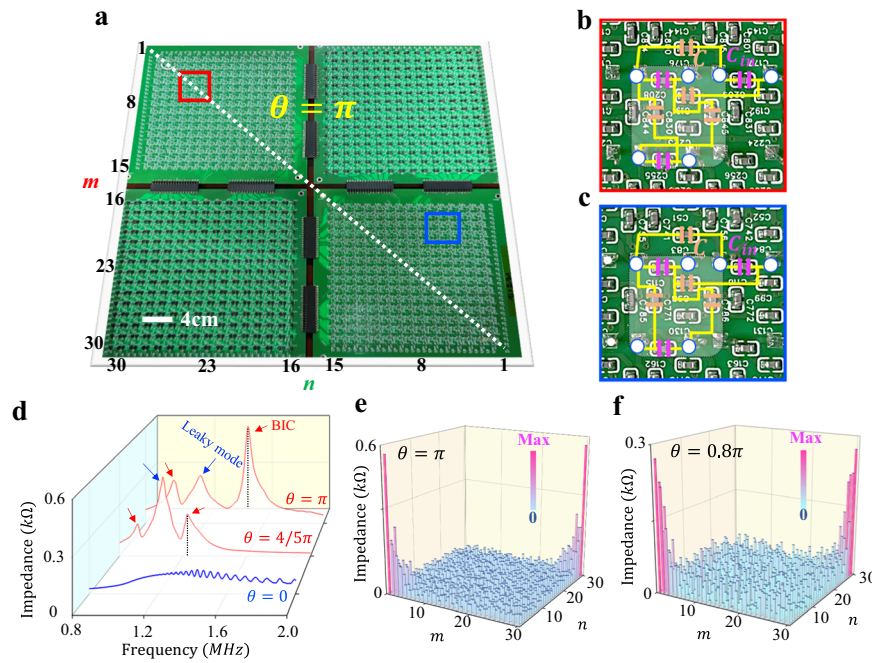


**Fig. 5 Experimental results for simulating anyonic bound states in the continuum (BICs).** **a** The Photograph image of fabricated circuit simulator with  $\theta = \pi$ . The white dash line marks the diagonal of the circuit sample. Red and blue blocks enclose the diagonal and non-diagonal regions of the circuit. **b** and **c** Enlarged views of the fabricated circuit around and far away from the diagonal. Red and pink capacitors correspond to  $C$  and  $C_{in}$ . **d** The measured frequency-dependent impedance at the corner node (1,1) with  $\theta = \pi$ ,  $0.8\pi$  and  $0$ . **e** and **f** The measured impedance profiles for the two-pseudofermion circuit simulator at 1.448 MHz and the two-anyon circuit simulator with  $\theta = 0.8\pi$  at 1.224 MHz. The color bars quantify the absolute value of measured impedances.

To experimentally simulate the anyonic BICs, designed 2D circuit simulators with  $\theta = 0$ ,  $\theta = 0.8\pi$  and  $\theta = \pi$  are fabricated, where the corresponding parameters are the same to those used in Fig. 4. A photograph image of the circuit sample with  $\theta = \pi$  is presented in Fig. 5a. Here, four printed circuit boards (PCBs), where each one contains  $15 \times 15$  node pairs, are applied for the circuit simulator. Enlarged views of the circuit around diagonals (enclosed by red block in Fig. 5a) and far away from diagonals (enclosed by the blue block in Fig. 5a) are plotted in Fig. 5b and c, respectively. It is shown that two circuit nodes connected by the capacitor  $C_{in}$  (plotted in pink) are considered to form an effective lattice site. Voltages at these two nodes are defined by  $V_{i,1}$  and  $V_{i,2}$ , which could be suitably formulated to construct a voltage pseudospin ( $V_{\downarrow i} = V_{i,1} - V_{i,2}$ ) for realizing required site couplings. To simulate the real-valued hopping rate, two capacitors ( $C$ ) labeled by orange symbols are used to directly link adjacent nodes without a cross. For the realization of the hopping rate with a direction-dependent phase factor ( $e^{\pm i\pi}$ ), two pairs of adjacent nodes are connected crossly via the capacitor  $C$ . Each node is grounded by an inductor  $L_g$  in the back side of the PCB. In addition, the tolerance of the circuit element is  $<1\%$  to avoid the detuning of circuit responses. Details of the sample fabrication are provided in Methods.

As shown by the red line in Fig. 5d, we measure the frequency-dependent impedance response at the corner node (1,1) of the fabricated two-pseudofermion circuit simulator. We can see that two significant impedance peaks (marked by red arrows) appear at 0.992 MHz and 1.488 MHz, being consistent to the simulation result of anyonic BICs in Fig. 4b. The central peak (the blue arrow) at 1.167 MHz correspond to the two-anyon leaky mode with a large IPR marked by the blue line in Fig. 2a. The larger width of measured impedance peaks results from the loss effect in the fabricated circuit. To fit the strength of loss in the fabricated

circuit, we calculate the frequency-dependent impedances with different series resistances of inductors (see Supplementary Note 4). We find that the effective series resistance of inductance in the fabricated circuit is  $\sim 150m\Omega$ . In addition, the spatial impedance distribution of the circuit at 1.448 MHz is further measured, as shown in Fig. 5e. We can see that the concentrated impedance profile is in a good consistency with the anyonic BIC of two pseudofermions.

Then, we turn to the fabricated circuit with  $\theta = 0.8\pi$  (see Supplementary Fig. 2 for the photograph of the sample). Here, the fabricated circuit simulator also contains  $30 \times 30$  node groups, which are large enough to ensure the exponential localization of anyonic BICs. The measured impedance spectrum of the circuit node (1,1) is shown in Fig. 5d. We can see that frequencies of two impedance peaks (0.914 MHz and 1.224 MHz marked by red arrows) are matched to the positive and negative energies of anyonic BICs with  $\theta = 0.8\pi$ . The spatial distribution of measured impedance profile at 1.224 MHz is displayed in Fig. 5f, where a good consistency to the profile of the anyonic BIC is also observed. The central peak at 1.036 MHz (marked by the blue arrow) corresponds to the leaky two-anyon mode with a large IPR.

Finally, we measure the impedance response of the circuit simulator for two bosons. It is found that no large impedance peak appears, indicating that the strongly localized eigenstate does not exist for two bosons. These experimental results are consistent with the theoretical prediction, and clearly demonstrate the effectiveness on the simulation of statistics-induced anyonic BICs.

## Conclusion

In conclusion, we discover a mechanism to generate BICs relying only on the quantum statistics. Based on analytical derivations and

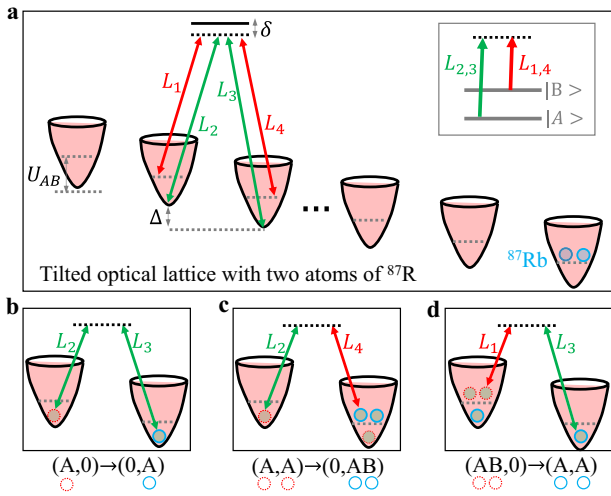


**Fig. 6 Realization of two-body anyonic bound states in the continuum (BICs) assisted by Raman tunneling.** **a** The Raman scheme for the realization of two-anyon BICs by two  $^{87}\text{Rb}$  atoms. **b–d** Raman-assisted hoppings in the form of  $(A,0) \rightarrow (0,A)$ ,  $(A,A) \rightarrow (0,AB)$ , and  $(AB,0) \rightarrow (A,A)$ . Red and blue circles correspond to initial and final states of two atoms.

numerical calculations, we find that two-anyon BICs can perfectly concentrate on the boundary of the 1D lattice without the existence of any impurity potentials when the statistical angle of two non-interacting anyons is beyond a threshold. By mapping eigenstates of two anyons to modes of designed electric circuits, anyonic BICs are effectively simulated by measuring impedance responses in frequency and spatial domains. Specifically, we fabricate three electric circuit networks with  $\theta = 0$ ,  $\theta = 0.8\pi$  and  $\theta = \pi$ , and find that the significant spatial localization of the impedance only appears in the circuit simulators with  $\theta = 0.8\pi$  and  $\theta = \pi$ , being consistent with the theoretical prediction that there is a threshold of  $\theta$  to trigger the formation of two-anyon BICs.

In addition, it is worth noting that our proposed anyonic BICs may also be realized in some quantum platforms<sup>32–34,55–59</sup>. For example, anyonic excitations can be created by bosons with occupation-dependent hopping amplitudes, which can be realized by assisted Raman tunneling<sup>32</sup>. Fig. 6a presents the schematic diagram for the realization of two-body anyonic BICs, where two  $^{87}\text{Rb}$  atoms locate in a tilted 1D optical lattice with open boundaries. The energy offset  $\Delta$  between neighboring sites is much larger than the lattice hopping  $J$  in the absence of tilting, making the direct hopping in the tilted lattice become ignored. Here, we consider two hyperfine states  $|A\rangle = |F=1, m_F=-1\rangle$  and  $|B\rangle = |F=2, m_F=-2\rangle$  of each  $^{87}\text{Rb}$  atom. In this case, four lasers  $L_{1,2,3,4}$  ( $L_1$ ,  $L_4$  and  $L_2$ ,  $L_3$  have the linear and circular polarizations, respectively) can be used to couple two states of  $^{87}\text{Rb}$ . As demonstrated by previous work<sup>59</sup>, we can assume in a very good approximation that the state  $|B\rangle$  and  $|A\rangle$  are only coupled with  $L_1$ ,  $L_4$  and  $L_2$ ,  $L_3$ , respectively, as shown in the inset of Fig. 6a.

We can use four lasers with frequencies being  $\omega_{1,2,3,4}$  to induce three types of Raman-assisted hoppings of two  $^{87}\text{Rb}$  atoms that are required to realize anyonic BICs. The first one is the transition  $(A,0) \rightarrow (0,A)$  with an energy shift  $\Delta E = -\Delta$ , as shown in Fig. 6b. Such a transition can be induced by  $L_2$  and  $L_3$  with  $\omega_2 - \omega_3 = -\Delta$ . As shown in Fig. 6c, the second transition  $(A,A) \rightarrow (0,AB)$  with  $\Delta E = -\Delta + U_{AB}$  can be induced by  $L_2$  and  $L_4$  with  $\omega_2 - \omega_4 = -\Delta + U_{AB}$ . The third one  $(AB,0) \rightarrow (A,A)$  with  $\Delta E = -\Delta - U_{AB}$  shown Fig. 6d is induced by  $L_1$  and  $L_3$  with  $\omega_1 - \omega_3 = -\Delta - U_{AB}$ .  $U_{AB}$  characterizes the interaction between  $|A\rangle$  and  $|B\rangle$  states of two atoms. It is worth noting that

the undesired Raman processes of  $(A,0) \rightarrow (0,B)$ ,  $(A,A) \rightarrow (0,AA)$  and  $(AA,0) \rightarrow (A,A)$  can be kept out of resonance by setting  $U_{AA} \gg W$  (the width of the Raman resonance). Under the above condition, the two-atom model with each atom having two states is reduced to a 1D single-component bosonic model. The on-site Fock states  $|0\rangle$ ,  $|1\rangle$  and  $|2\rangle$  correspond to  $|0\rangle$ ,  $|A\rangle$  and  $|AB\rangle$ . By setting the Rabi frequency of the laser  $L_j$  to  $\Omega_j e^{i\Phi_j}$  with  $\Phi_1 = -\Phi$ ,  $\Phi_{2,3,4} = 0$  and  $|\Omega_1||\Omega_4|/4 = |\Omega_2||\Omega_3|/3 = |\Omega_1||\Omega_3|/2\sqrt{3} = |\Omega_2||\Omega_4|/2\sqrt{3} = \Omega_1^2|\Omega_4|/4 = |\Omega_2||\Omega_3|/3 = |\Omega_1||\Omega_3|/2\sqrt{3} = |\Omega_2||\Omega_4|/2\sqrt{3} = \Omega^2$ <sup>59</sup>, we can obtain the effective Hamiltonian with occupation-dependent Peierls phase as  $H_{\text{eff}} = -0.5J\Omega^2/(\Delta\delta) \sum_j (\hat{b}_j^+ e^{i\Phi n_j} \hat{b}_{j+1} + H.c.)$  with  $\delta$  being the detuning from the single-photon transitions ( $\delta \gg U_{AB}, \Delta, \Omega$ ).  $b_j^+$  ( $b_j$ ) are creation (annihilation) operators at site  $j$ , and  $\hat{n}_j = \hat{b}_j^+ \hat{b}_j$ . Based on the fractional version of a Jordan–Wigner transformation  $\hat{a}_j = \hat{b}_j e^{i\Phi \sum_{l=1}^{j-1} \hat{n}_l}$ , the effective Hamiltonian  $H_{\text{eff}}$  is transformed to the two-anyon lattice model of Eq. (1) with  $\hat{a}_j$  ( $\hat{a}_j^+$ ) satisfying the anyonic statistics ( $\Phi$  is the anyonic statistical angle).

There are also many open questions related to anyonic BICs remained to be solved. For example, inspired by novel properties of three-boson states in Hubbard model<sup>60</sup> and two-boson topological states in two dimensions<sup>61</sup>, it would be very interesting to investigate the 1D anyonic system with three or more anyons and two-anyon systems in two dimensions to see what novel phenomena related to anyonic BICs appear. And, following a recent experiment on the demonstration of nonlinearity-induced two-boson topological states with microwave qubits<sup>62</sup>, the study of influences by non-Hermitian, non-linear and topological effects on the anyonic BICs is also very interesting. These studies will shed more light on the novel physics of correlated BICs, and can also suggest a useful way to construct classical BICs in high dimensions.

## Methods

**Sample fabrications and circuit signal measurements.** We exploit the 2D electric circuits by using PAD program software, where the PCB composition, stack-up layout, internal layer and grounding design are suitably engineered. Here, the well-designed 2D PCB possesses six layers, containing the top layer, the bottom layer, two mid-layers, and two internal planes, to suitably arrange circuit elements, linking wires and the ground setting. It is worth noting that the ground layer should be placed in the gap between any two layers to avoid the mutual inductance. Moreover, all PCB traces have a relatively large width (0.75 mm) to reduce the parasitic inductance, and the spacing between electronic devices is also large enough (0.3–0.5 mm) to avert spurious inductive coupling. The SMP connectors are welded on PCB nodes for the signal injection and detection. To ensure the realization of anyonic BICs in electric circuits, both the tolerance of circuit elements and series resistance of inductors should be as low as possible. For this purpose, we use a WK6500B impedance analyzer to select circuit elements with a high accuracy (the averaged disorder strength is <1%) and low losses.

**Circuit simulations and numerical calculations.** Our analytical theory on anyonic BICs is based on the Bethe-type ansatz of two-anyon eigenstates. Detailed derivations are given in Supplementary Materials. The matrix diagonalizations, which are used to calculate eigen-spectra and associated eigenmodes of two anyons, are completed in MATLAB interface. The numerical accuracy is high enough to ensure convergence. All circuit simulations are performed in LTSpice software.

## Data availability

All data are displayed in the main text and Supplementary Information. The data that support the findings of this study are available from the corresponding author upon reasonable request.

## Code availability

The code that supports the plots within this paper are available from the corresponding author upon reasonable request.



Received: 19 January 2023; Accepted: 22 May 2023;

Published online: 13 June 2023

## References

1. von Neuman, J. & Wigner, E. Über merkwürdige diskrete Eigenwerte. Über das Verhalten von Eigenwerten bei adiabatischen Prozessen. *Phys. Z.* **30**, 467–470 (1929).
2. Hsu, C. W., Zhen, B., Stone, A. D., Joannopoulos, J. D. & Soljačić, M. Bound states in the continuum. *Nat. Rev. Mater.* **1**, 16048 (2016).
3. Koshelev, K., Bogdanov, A. & Kivshar, Y. Meta-optics and bound states in the continuum. *Sci. Bull.* **64**, 836–842 (2019).
4. Marinica, D. C., Borisov, A. G. & Shabanov, S. V. Bound states in the continuum in photonics. *Phys. Rev. Lett.* **100**, 183902 (2008).
5. Plotnik, Y. et al. Experimental observation of optical bound states in the continuum. *Phys. Rev. Lett.* **107**, 183901 (2011).
6. Xiao, Y., Ma, G., Zhang, Z.-Q. & Chan, C. T. Topological subspace induced bound states in continuum. *Phys. Rev. Lett.* **118**, 166803 (2017).
7. Cerjan, A. et al. Observation of a higher-order topological bound state in the continuum. *Phys. Rev. Lett.* **125**, 213901 (2020).
8. Ardizzone, V. et al. Polariton Bose–Einstein condensate from a bound state in the continuum. *Nature* **605**, 447–452 (2022).
9. Hsu, C. W. et al. Observation of trapped light within the radiation continuum. *Nature* **499**, 188–191 (2013).
10. Zhen, B., Hsu, C. W., Lu, L., Stone, A. D. & Soljačić, M. Topological nature of optical bound states in the continuum. *Phys. Rev. Lett.* **113**, 257401 (2014).
11. Kodigala, A. et al. Lasing action from photonic bound states in continuum. *Nature* **541**, 196–199 (2017).
12. Monticone, F. & Alù, A. Embedded photonic eigenvalues in 3D nanostructures. *Phys. Rev. Lett.* **112**, 213903 (2014).
13. Zhang, Y. et al. Observation of polarization vortices in momentum space. *Phys. Rev. Lett.* **120**, 186103 (2018).
14. Doeleman, H. M., Monticone, F., den Hollander, W., Andrea, A. & Koenderink, A. F. Experimental observation of a polarization vortex at an optical bound state in the continuum. *Nat. Photon.* **12**, 397–401 (2018).
15. Minkov, M. et al. Zero-index bound states in the continuum. *Phys. Rev. Lett.* **121**, 263901 (2018).
16. Azzam, S. I., Shalae, V. M., Boltasseva, A. & Kildishev, A. V. Formation of bound states in the continuum in hybrid plasmonic-photonic systems. *Phys. Rev. Lett.* **121**, 253901 (2018).
17. Jin, J. et al. Topologically enabled ultrahigh-Q guided resonances robust to out-of-plane scattering. *Nature* **574**, 501–504 (2019).
18. Yin, X. et al. Observation of topologically enabled unidirectional guided resonances. *Nature* **580**, 467–471 (2020).
19. Stillinger, F. H. & Herrick, D. R. Bound states in the continuum. *Phys. Rev. A* **11**, 446–454 (1975).
20. Molina, M. I., Miroschnichenko, A. E. & Kivshar, Y. S. Surface bound states in the continuum. *Phys. Rev. Lett.* **108**, 070401 (2012).
21. Corrielli, G., Della Valle, G., Crespi, A., Osellame, R. & Longhi, S. Observation of surface states with algebraic localization. *Phys. Rev. Lett.* **111**, 220403 (2013).
22. Hwang, M. S. et al. Ultralow-threshold laser using super-bound states in the continuum. *Nat. Commun.* **12**, 4135 (2021).
23. Huang, C. et al. Ultrafast control of vortex microlasers. *Science* **367**, 1018–1021 (2020).
24. Zhang, J. M., Braak, D. & Kollar, M. Bound states in the continuum realized in the one-dimensional twoparticle Hubbard model with an impurity. *Phys. Rev. Lett.* **109**, 116405 (2012).
25. Longhi, S. & Valle, Della G. Tamm–Hubbard surface states in the continuum. *J. Phys. Condens. Matter* **25**, 235601 (2013).
26. Leinaas, J. & Myrheim, J. On the theory of identical particles. *Nuovo Cim. B* **37**, 1–23 (1977).
27. Wilczek, F. Magnetic flux, angular momentum, and statistics. *Phys. Rev. Lett.* **48**, 1144–1146 (1982).
28. Canright, G. S. & Girvin, S. M. Fractional statistics: quantum possibilities in two dimensions. *Science* **247**, 1197–1205 (1990).
29. Haldane, F. D. M. ‘Fractional statistics’ in arbitrary dimensions: a generalization of the Pauli principle. *Phys. Rev. Lett.* **67**, 937–940 (1991).
30. Kundu, A. Exact solution of double  $\delta$  function Bose gas through an interacting anyon gas. *Phys. Rev. Lett.* **83**, 1275 (1999).
31. Kitaev, A. Anyons in an exactly solved model and beyond. *Ann. Phys. (Amst.)* **321**, 2 (2006).
32. Keilmann, T. et al. Statistically induced phase transitions and anyons in 1D optical lattices. *Nat. Commun.* **2**, 361 (2011).
33. Bartolomei, H. et al. Fractional statistics in anyon collisions. *Science* **368**, 173–177 (2020).
34. Nakamura, J., Liang, S., Gardner, G. C. & Manfra, M. Direct Observation of anyonic braiding statistics. *Nat. Phys.* **16**, 931–936 (2020).
35. Batchelor, M. T., Guan, X.-W. & Oelkers, N. One-dimensional interacting anyon gas: low-energy properties and Haldane exclusion statistics. *Phys. Rev. Lett.* **96**, 210402 (2006).
36. Kim, E.-A., Lawler, M., Vishveshwara, S. & Fradkin, E. Jordan–Wigner Transformation for Quantum-Spin Systems in Two Dimensions and Fractional Statistics. *Phys. Rev. Lett.* **95**, 176402 (2005).
37. Kitaev, A. Y. Fault-tolerant quantum computation by anyons. *Ann. Phys. (Amst.)* **303**, 2 (2003).
38. Longhi, S. & Della Valle, G. Anyonic Bloch oscillations. *Phys. Rev. B* **85**, 165144 (2012).
39. Zhang, W. et al. Observation of Bloch oscillations dominated by effective anyonic particle statistics. *Nat. Commun.* **13**, 2392 (2022).
40. Olekhno, N. et al. Topological transitions driven by quantum statistics and their electrical circuit emulation. *Phys. Rev. B* **105**, 205113 (2022).
41. Thouless, D. J. Electrons in disordered systems and the theory of localization. *Phys. Rep.* **13**, 93 (1974).
42. Benalcazar, W. A. & Cerjan, A. Bound states in the continuum of higher-order topological insulators. *Phys. Rev. B* **101**, 161116(R) (2020).
43. Olekhno, N. A. et al. Experimental realization of topological corner states in long-range-coupled electrical circuits. *Phys. Rev. B* **105**, L081107 (2022).
44. Ning, J., Owens, C., Sommer, A., Schuster, D. & Simon, J. Time and site resolved dynamics in a topological circuit. *Phys. Rev. X* **5**, 021031 (2015).
45. Albert, V. V., Glazman, L. I. & Jiang, L. Topological properties of linear circuit lattices. *Phys. Rev. Lett.* **114**, 173902 (2015).
46. Lee, C. et al. Topoelectrical circuits. *Commun. Phys.* **1**, 39 (2018).
47. Imhof, S. et al. Topoelectrical-circuit realization of topological corner modes. *Nat. Phys.* **14**, 925 (2018).
48. Zhang, W. et al. Experimental observation of higher-order topological Anderson insulators. *Phys. Rev. Lett.* **126**, 146802 (2021).
49. Olekhno, N. et al. Topological edge states of interacting photon pairs realized in a topoelectrical circuit. *Nat. Commun.* **11**, 1436 (2020).
50. Yu, R., Zhao, Y. & Schnuder, A. P. 4D spinless topological insulator in a periodic electric circuit. *Natl. Sci. Rev.* **7**, nwa065 (2020).
51. Wang, Y., Price, H. M., Zhang, B. & Chong, Y. D. Circuit realization of a four-dimensional topological insulator. *Nat. Commun.* **11**, 2356 (2020).
52. Helbig, T. et al. Generalized bulk–boundary correspondence in non-Hermitian topoelectrical circuits. *Nat. Phys.* **16**, 747 (2020).
53. Liu, S. et al. Non-Hermitian Skin Effect in a Non-Hermitian Electrical Circuit. *Research* **2021**, 5608038 (2021).
54. Zhang, W., Yuan, H., Sun, N., Sun, H. & Zhang, X. Observation of novel topological states in hyperbolic lattices. *Nat. Commun.* **13**, 2937 (2022).
55. Mills, S. M., Averin, D. V. & Du, X. Localizing fractional quasiparticles on graphene quantum Hall antidots. *Phys. Rev. Lett.* **125**, 227701 (2020).
56. Lu, C.-Y. et al. Demonstrating anyonic fractional statistics with a six-qubit quantum simulator. *Phys. Rev. Lett.* **102**, 030502 (2009).
57. Cho, Y., Angelakis, D. G. & Bose, S. Fractional Quantum Hall State in Coupled Cavities. *Phys. Rev. Lett.* **101**, 246809 (2008).
58. Todoric, M., Jukić, D., Radić, D., Soljačić, M. & Buljan, H. Quantum Hall Effect with Composites of Magnetic Flux Tubes and Charged Particles. *Phys. Rev. Lett.* **120**, 267201 (2018).
59. Greschner, S. & Santos, L. Anyon Hubbard model in one-dimensional optical lattices. *Phys. Rev. Lett.* **115**, 053002 (2015).
60. Zhong, J. & Poddubny, A. N. Classification of three-photon states in waveguide quantum electrodynamics. *Phys. Rev. A* **103**, 023720 (2021).
61. Stepanenko, A. A., Lyubarov, M. D. & Gorlach, M. A. Higher-Order Topological Phase of Interacting Photon Pairs. *Phys. Rev. Lett.* **128**, 213903 (2022).
62. Besedin, I. S. et al. Topological excitations and bound photon pairs in a superconducting quantum metamaterial. *Phys. Rev. B* **103**, 224520 (2021).

## Acknowledgements

This work is supported by the National Key R & D Program of China No. 2022YFA1404900 and the National Natural Science Foundation of China No.12104041.

## Author contributions

W.Z. finished the theoretical investigation on anyonic BICs with the help of L.Q. L.Q. finished the experiments with the help of H.S., W.Z., and X.Z. wrote the paper. X.Z. initiated and designed this research project.

## Competing interests

The authors declare no competing interests.

**Additional information**

**Supplementary information** The online version contains supplementary material available at <https://doi.org/10.1038/s42005-023-01245-6>.

**Correspondence** and requests for materials should be addressed to Xiangdong Zhang.

**Peer review information** *Communications Physics* thanks the anonymous reviewers for their contribution to the peer review of this work. A peer review file is available.

**Reprints and permission information** is available at <http://www.nature.com/reprints>

**Publisher's note** Springer Nature remains neutral with regard to jurisdictional claims in published maps and institutional affiliations.



**Open Access** This article is licensed under a Creative Commons Attribution 4.0 International License, which permits use, sharing, adaptation, distribution and reproduction in any medium or format, as long as you give appropriate credit to the original author(s) and the source, provide a link to the Creative Commons licence, and indicate if changes were made. The images or other third party material in this article are included in the article's Creative Commons licence, unless indicated otherwise in a credit line to the material. If material is not included in the article's Creative Commons licence and your intended use is not permitted by statutory regulation or exceeds the permitted use, you will need to obtain permission directly from the copyright holder. To view a copy of this licence, visit <http://creativecommons.org/licenses/by/4.0/>.

© The Author(s) 2023